at the least cost. Uniform pesticide regulation may be much more costly than fees in attaining policy targets. Furthermore, when the health costs of risk can be enumerated, the most efficient fee or tax policies are those that equate the incremental benefits of risk reduction to the incremental costs of reduced economic activities. It is advisable to use the proceeds of pesticide-use fees or taxes to finance R&D efforts when developing alternative pest-management practices, subsidizing their adoption, and addressing negative side effects from pesticide use.

Establishing mechanisms for monitoring and enforcing environmental regulations has always been an administrative challenge. The organizations established to implement pesticide registration requirements in some states (most notably, California) provide the base to administer pesticide taxation policies. The derivation and assessment of policy parameters will require much more "policy-relevant" research and more interdisciplinary cooperation among managerial, agricultural, and environmental health scientists.

REFERENCES AND NOTES

1. D. Zilberman and J. B. Siebert, Eds., *Economic Perspectives on Pesticide Use in California* (Working Paper 564, Department of Agricultural and Resource Economics, University of California, Berkeley, 1990).
2. G. A. Carlson in (*1*), chap. 3.
3. C. Carrasco-Tauber in (*1*), chap. 6.
4. E. Lichtenberg, D. D. Parker, D. Zilberman in (*1*), chap. 7.
5. N. C. Toscano, K. Kido, C. Giorgio, unpublished paper.
6. R. E. Just, D. L. Hueth, A. Schmitz, *Applied Welfare Economics and Public Policy* (Prentice-Hall, Englewood Cliffs, NJ, 1982).
7. F. G. Zalom and J. F. Strand, *Calif. Agric.* **44**, 16 (1990).
8. J. A. Hewitt, S. O. Archibald, S. J. Moss, "A short-run welfare analysis of pesticide bans in California agriculture" (Food Research Institute Working Paper, Stanford University, 1991); D. Pimentel, unpublished paper; GRC Economics, unpublished paper.
9. For this high value, it is assumed that the impact is distributed normally and is the 95th percentile of the outcome distribution.
10. R. D. Knutson, C. R. Taylor, J. B. Penson, Jr., E. G. Smith, *Economic Impacts of Reduced Chemical Use* (Knutson & Associates, College Station, TX, 1990).
11. H. Ayer and N. Conklin, *Choices* **4**, 24 (1990).
12. E. Lichtenberg and D. Zilberman, *Am. Econ. Rev.* **76**, 1135 (1986).
13. L. Richardson, *Calif. Farmer* **273**, 2 (1990).
14. S. L. Ott, *Agribusiness* **6**, 593 (1990).
15. U.S. Department of Agriculture, ERS, *Food Rev.* **14**, 1 (1991), p. 43.
16. E. Lichtenberg and D. Zilberman, in (*1*), chap. 12.
17. E. Lichtenberg, R. C. Spear, D. Zilberman, in (*1*), chap. 11.
18. U.S. Department of Agriculture, 1990 Chartbook, *Agriculture Handbook No. 689* (Washington, DC, 1990).

19. This study was supported in part by the Environmental Protection Agency. We gratefully acknowledge editorial assistance from A. Nolan, M. R. Graham, and H. C. Schmitz. Giannini Foundation Paper no. 989.

Numerical Models of Extragalactic Radio Sources

JACK O. BURNS, MICHAEL L. NORMAN, DAVID A. CLARKE

Numerical simulations with supercomputers allow analysis of the wide range of nonlinear physics inherent in the hydrodynamic and magnetohydrodynamic equations. When applied to extragalactic radio sources, these numerical models have begun to reproduce many of the complex structures observed on telescopic images. This combination of telescopic and numerical observations provides powerful probes of the physics of radio galaxies. In this review, some of the recent results from both two-dimensional and three-dimensional numerical simulations of the formation and evolution of extended radio morphologies are described. These numerical models have allowed the exploration of important physical phenomena including the role of magnetic fields in the dynamics and emissivity of extended radio galaxies, intermittent outflow from the cores of active galaxies, instabilities and disruption of fluid jets, and the bending of collimated outflows by motion through the intergalactic medium.

DURING THE LAST DECADE, REMARKABLE PROGRESS HAS been made in imaging extragalactic radio sources by means of aperture synthesis telescopes such as the Very Large Array (VLA) (*1*). High-fidelity radio maps reveal a wealth of complex structures (*2*), including twin lobes of emission on opposite sides of an active galactic nucleus (AGN), collimated jets stretching between the galaxy core and the lobes, and knots (or hot spots) and filaments within the lobes and jets.

During this same decade, significant progress was also made in the theoretical interpretation of these radio morphologies. Much of this advance resulted from the increased accessibility of large-scale supercomputer-class machines and the advent of hydrodynamic and magnetohydrodynamic (MHD) algorithms of advanced design. These coupled with the National Science Foundation computer network and powerful yet affordable computer workstations permit a broad cross section of the astronomical community to participate in numerical simulations and interpretations of extragalactic radio sources. For many years, the national observatories provided an infrastructure that resulted in high-quality data for both the expert and the novice. In much this same way, the national supercomputer centers now permit observers as well as theorists to participate in sophisticated modeling of astronomical phenomena.

J. O. Burns is head of the Astronomy Department, Box 30001, Department 4500, New Mexico State University, Las Cruces, NM 88003. M. L. Norman and D. A. Clarke are with the National Center for Supercomputing Applications, University of Illinois at Urbana-Champaign, Urbana, IL 61801.

Observed Radio Source Characteristics

The typical structures associated with powerful extragalactic radio sources are illustrated in Fig. 1, A and B. The frequency spectrum

of these radio sources is well represented by a power law in the form $S_\nu \propto \nu^{-\alpha}$, where S_ν is the flux density at frequency ν and α is the spectral index. This fact, combined with the observation of high degrees of linear polarization ($\leq$70%) in the radio lobes, strongly suggests that the emission is synchrotron radiation (*3*). Such radiation is produced by relativistic electrons (Lorentz scale factor $\gamma \sim 1000$) spiraling in magnetic fields (typically, 10 to 100 μG). The observed Faraday rotation and depolarization in many sources may further indicate that these fast particles are embedded within a thermal plasma.

Extragalactic radio sources can be divided into two classes according to their power and morphology (*4*). Class II sources were the first to be imaged by early radio telescopes because of their higher radio powers ($>10^{25}$ W/Hz at 1.4 GHz). They are characterized by a "classical double" morphology (Fig. 1). A compact core, optically identified with a galaxy or quasar, lies between two "lobes" of emission. The radio surface brightness peaks at "hot spots" located at the extremities of the lobes. A single "jet" is most often found pointing toward one of the lobes. These jets have been interpreted as collimated supersonic outflows of plasma (including relativistic particles, magnetic field, and thermal gas) initially formed near the nuclear engine (*5*). It is curious that, although there are symmetrical lobes on either side of the AGN, there is generally only one jet visible. One possible explanation involves a relativistic beaming effect (*6*). If the bulk velocity of plasma in the jet is relativistic, then the flux density of the jet pointed toward the observer is Doppler-boosted and the counterjet is similarly diminished by the same factor, thus producing potentially large asymmetries between the jets. In principle, higher contrast radio images should reveal the presence of counterjets if this model is correct. We are beginning to see possible pieces but no complete counterjets as of yet (*7–9*). The jets in classical doubles also are remarkably well collimated (with opening angles of less than a few degrees) and have projected magnetic fields oriented parallel to the jet axis.

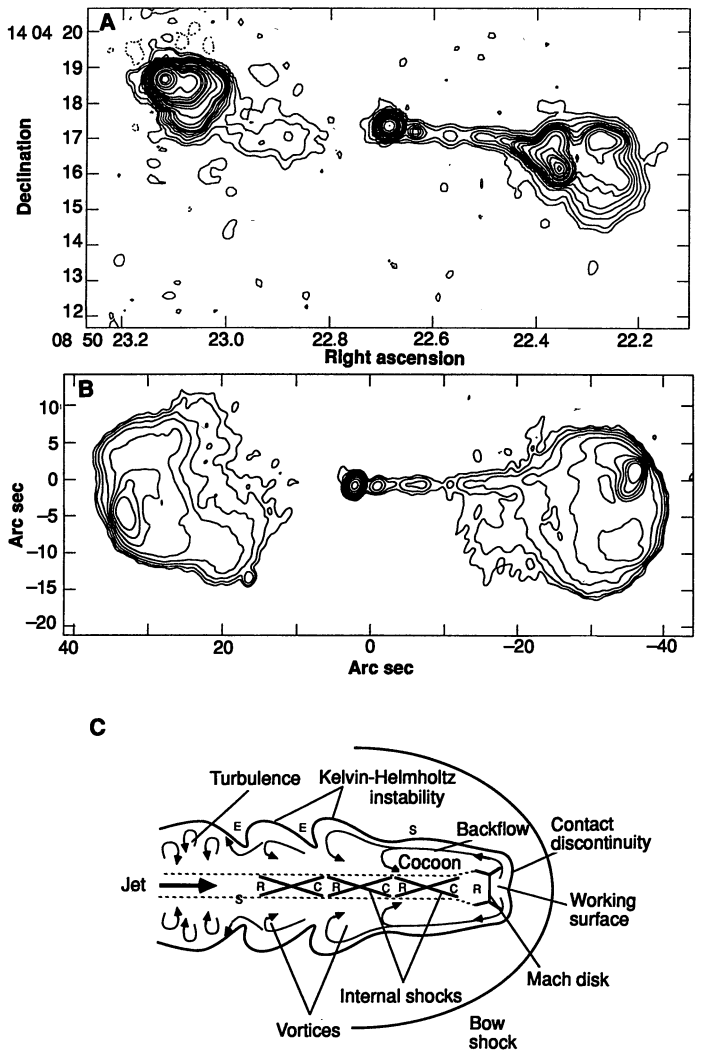

Fig. 1. Observations and a schematic model of classical double radio sources. (**A** and **B**) VLA images at 6-cm wavelength of radio quasars 3C 208 (*7*) and 3C 47 (*8*). (**C**) A "cartoon" illustration of the standard model of classical doubles based on numerical simulations. R and C are rarefaction and compression zones, respectively; S denotes a shear surface; E is a turbulent eddy.

Class I sources are less luminous but are more abundant and more complex in their structure. These sources are virtually always identified with galaxies, some of which are in clusters. These cluster sources, in particular, are often termed "tailed" radio galaxies because they are bent and edge-darkened [that is, emission trails off away from the compact core (see below)]. Most often, two symmetrical jets appear emanating from the galaxy nucleus. In sources located in galaxy clusters, the jets or tails are often bent via ram pressure ($\rho_{IGM} V_{gal}^2$, where ρ_{IGM} is the density of the intergalactic medium, IGM, and V_{gal} is the galaxy velocity) produced by galaxy motion (>500 km s^{-1} in rich clusters) through a dense IGM. This medium is directly detected via its thermal bremsstrahlung x-ray emission (*10*). The jets in class I sources generally have larger opening angles than jets in class II sources and a projected **B** field that is oriented perpendicular to the jet (possibly a projected toroidal field).

A Model of Classical Double Radio Sources

It is generally assumed that the jets in extragalactic radio sources originate from the vicinity of a large (10^7 to 10^9 solar masses), rotating black hole. Such compact objects are the most efficient mechanism known for converting gravitational potential energy into bulk outflow and radiation. An electron-positron beam, for example, can be extracted along the rotation axis of the black hole and collimated via an electrodynamic dynamo process operating in a surrounding accretion disk (*11*). This beam then propagates through the interstellar medium (ISM), and eventually through the IGM. During the travels of the jet, the turbulent region around the jet (cocoon) will likely entrain significant amounts of thermal gas from the ambient medium (*12*). The interaction of the jet with the external gas plays an important role in determining the morphology of the radio source as discussed below. Our primary concern in this review is with the subsequent evolution of the jet and radio lobe.

Because the Larmor radii of the particles in the jet and lobe are much less than the typical scale sizes of the radio features, one can use a fluid approximation to model these structures. In its simplest form, where viscosity and thermal conductivity are ignored, the fluid motion is governed by Euler's conservation laws of mass, momentum, and energy, along with an adiabatic equation of state (*13*). These equations are used as a starting point for studying the physics of extended radio morphologies. Moreover, ideal (that is, nonresistive) MHD effects are beginning to be incorporated into numerical simulations of radio jets. The computer program that our group has developed to solve these equations is called ZEUS (*14*). It runs on the Cray supercomputers at the National Center for Supercomputering Applications (NCSA). ZEUS is a finite difference scheme that solves the equations of ideal MHD on an Eulerian grid in time and space using a battery of robust numerical techniques. The algorithms used to solve the hydrodynamical equations are described by Norman and Winkler (*15*). The algorithm used to evolve the

magnetic field is a hybrid of the constrained transport scheme (*16*) and a method of characteristics (*17*). This has led to an extremely stable algorithm (for example, shear Alfvén waves), which preserves $\nabla \cdot \mathbf{B} = 0$ to within truncation errors.

Numerical simulations, coupled with earlier pioneering analytical work (*5*), have permitted astronomers to begin interpreting the basic features observed in extended radio galaxies. The twin-exhaust model of Blandford and Rees (*5*) proposed that a fluid beam propagating through the ambient gas could explain the edge-brightened double lobes and hot spots observed in class II sources. In later numerical studies (*18, 19*), three parameters were used to control the flow morphology. These are (i) the ratio of the jet density to the ambient density, $\eta = \rho_{jet}/\rho_{amb}$; (ii) the Mach number of the flow measured with respect to the internal jet sound speed, $M = V_{jet}/c_{jet}$; and (iii) the ratio of the pressure of the jet to that of the undisturbed ambient medium, $K = P_{jet}/P_{amb}$. The now "standard model" of classical doubles is illustrated in an idealized sketch in Fig. 1C. In Fig. 2, several different epochs are shown for the evolution of an axisymmetric cylindrical jet with $\eta = 0.1$, $M = 6$, and $K = 1$.

Most models of classical doubles assume that the bulk velocity of the jet is large and supersonic. For simplicity, we further assume in what follows that the outflow velocity is nonrelativistic (*20*). (However, as discussed above, relativistic jets may have important consequences for certain observed features.) This supersonic flow will drive a bow shock out in front of the jet. Generally, such a bow shock is not observed on radio images, suggesting that relativistic electrons or magnetic fields, or both, are not present in sufficient quantities in the ambient medium to illuminate the bow shock.

By balancing the ram pressures of the jet and the IGM, one can show that the advanced speed of the "working surface" or head of the jet is

$$V_{head} = \frac{V_{jet}\sqrt{\eta}}{1 + \sqrt{\eta}} \quad (1)$$

For light ($\eta \ll 1$) jets, the outflow must be decelerated near the leading edge. Hydrodynamically, this is accomplished by a strong planar shock or Mach disk. The bulk kinetic energy of the jet is thermalized as it passes through the Mach disk, creating a relatively compact region of high pressure downstream at the working surface identified with the radio hot spots.

The pressure difference between the working surface and the ram pressure of the IGM will drive a vigorous flow both sideways and back along the jet. This inflates a "cocoon" or wastebasket of subsonic jet debris surrounding the jet. The cocoon is separated from the shocked ambient gas by a contact discontinuity, which is a jump in the temperature but not the pressure. If the jet is initially hypersonic ($M \gg 1$), the strong bow shock will create a region of relatively high thermal pressure in the shocked ambient. Because the cocoon and the jet are in thermal pressure balance with the shocked ambient, the jet will appear to be overpressured with respect to the undisturbed IGM. This simple picture may explain the initially puzzling observations of quasar jets with internal pressures that exceed those inferred from x-ray observations of the hot IGM (*21*).

Figure 2 illustrates that the jet-lobe structure is dynamic. There is a quasi-periodic creation and shedding of large-scale vortices at the working surface. The Mach disk varies in position with respect to the bow shock; at times, the Mach disk even disappears and later reforms. Thus, a snapshot of the numerical radio source at a given epoch may look very different in detail from that at another epoch (although the gross double-lobe and jet structure is preserved). This dynamic nature probably explains in part why no two radio galaxies look exactly alike.

Outside the jet, the backflowing cocoon is turbulent. This turbulence is expected because the free shear surface separating the cocoon from the shocked ambient gas is subject to classical Kelvin-Helmholtz (K-H) fluid instabilities (*22*). One can see the amplitude of the waves grow as a function of distance from the working surface. This gives the lobes an irregular appearance as observed in most classical doubles (see Fig. 1).

These instabilities also have a direct impact on the internal structure of the jet. Perturbations imposed by the growth and saturation of K-H instabilities drive oblique shocks into the jet as the turbulent eddies contact the jet surface. In an axisymmetric jet, this produces a regular pattern of biconical shocks. It is reasonable to identify the regular pattern of knots observed in many luminous jets (see Fig. 1) with the biconical shocks seen in the numerical simulations.

Finally, an exploration through control parameter space (*23*) demonstrates that larger cocoons are produced by light, highly supersonic ($M > 10$) jets (*20*). This behavior is consistent with a

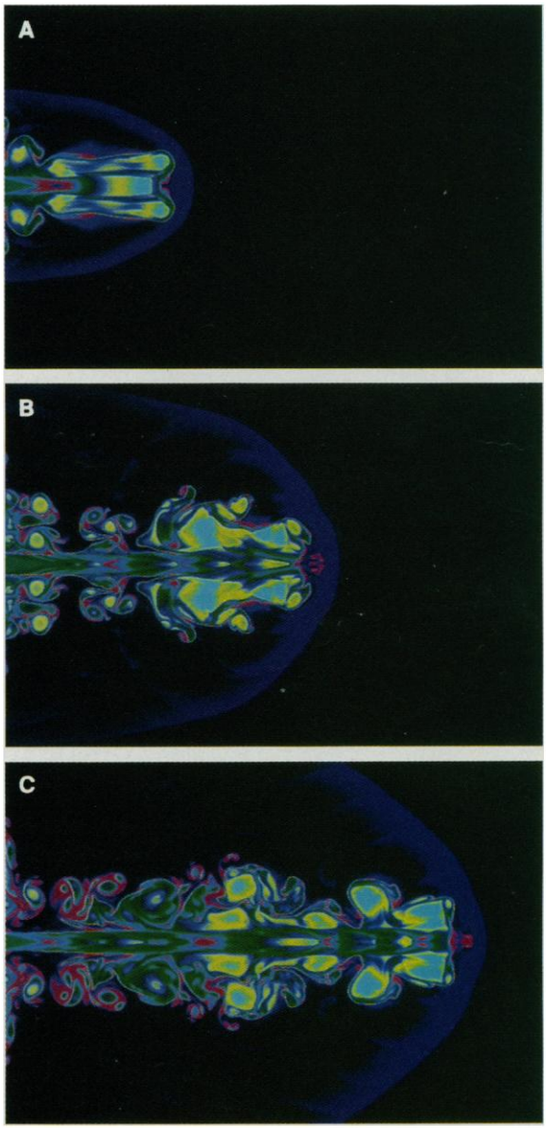

Fig. 2. Three epochs (**A** to **C**) in the evolution of an axisymmetric cylindrical jet in a classical double source with $\eta = 0.1$, $M = 6$, and $K = 1$. A pseudo-color representation of gas density is shown revealing a variety of flow structures within the jet as diagrammed in Fig. 1C. The flow is unsteady as vortices are shed at the working surface into the cocoon.

simple analysis of the transverse confinement of the cocoon by ram pressure. Near the working surface, the high thermal pressure cocoon will expand sideways with a velocity

$$V_{\text{cocoon}} = \left(\frac{P_{\text{head}}}{\rho_{\text{amb}}}\right)^{1/2} \quad (2)$$

This velocity is then proportional to the Mach number of the head with respect to the ambient sound speed. Ram pressure balance, then, reveals that

$$V_{\text{cocoon}} \propto \frac{M_{\text{jet}}}{1 + \sqrt{\eta}} \quad (3)$$

So, jets with low density and high Mach number will produce larger diameter cocoons or lobes. Because most classical double sources are observed to have broad, diffuse lobes, one infers from the numerical simulations that the jets in these sources are likely to be light and highly supersonic. This is an important insight because we have no direct way of measuring the velocity or density of the jet or lobe from the strictly continuum emission recorded by radio telescopes.

In summary, one can begin to make a direct association between the features observed on radio images with those predicted by the models as in Fig. 1. The jet is a supersonic fluid beam transporting relativistic particles, magnetic field, and thermal gas from the engine to the lobe. Compact hot spots are working surfaces where the jet decelerates and the plasma is thermalized at the Mach disk. The lobes are equivalent to the cocoons of jet waste material that are blown backwards by the strong ram pressure of the IGM.

MHD Jets

Although the hydrodynamical simulations of classical doubles reproduce many of the features seen on VLA radio maps, the inclusion of magnetic fields in the models is important for two reasons. First, it is possible that the magnetic fields play a role in the dynamics of the flow and thus the resulting morphology of extended radio sources. Second, the **B** fields are crucial in determining the radiation pattern from the flow. Up until now in this article, we have assumed that images of hydrodynamical variables such as density and pressure can be compared with VLA images to infer the physics of the underlying flow. However, a proper comparison (and true numerical "observations") would involve an emissivity image from the numerical simulations.

Recently, several major efforts have been made to include ideal MHD in two-dimensional (2-D) jet simulations (*24*). The strength of the magnetic field in these jets is most conveniently given by the ratio

$$\beta = \frac{P}{B^2/8\pi} \quad (4)$$

where P is the thermal pressure (nkT, where n is the density, k is the Boltzmann constant, and T is temperature). In the case of a dynamically active magnetic field ($\beta < 1$), the jet morphology is strikingly different from that of the hydrodynamical limit (Fig. 3). For such a magnetically confined jet, a Mach disk is found in roughly the same location as in the hydrodynamic (that is, $\beta \gg 1$) jet. However, the postshock jet material has now been confined by the $\mathbf{J} \times \mathbf{B}$ forces ($\mathbf{J}$ is current density) to form a "nose cone" that leads the Mach disk. No cocoon surrounds this "naked" jet. Both the jet and the nose cone are confined by the pressure of the toroidal magnetic field. This morphology has been confirmed by two independent numerical simulations that use different codes (*24*). This lobeless structure is very different from that of most classical doubles, like those in Fig. 1. One must conclude, therefore, that most luminous doubles, which contain extended lobes, do not have dynamically dominant magnetic fields.

Are there any radio sources that appear to have this nose cone morphology? The famous radio quasar 3C 273 shown in Fig. 3D may be one of a few possible examples. For the most part, the jet is naked and the forwardmost structure contains a spectral gradient (beyond the last prominent jet knot) suggesting aging electrons along its length, as one might expect if the last site of in situ electron reacceleration (*25*) occurs at the Mach disk. Another possible

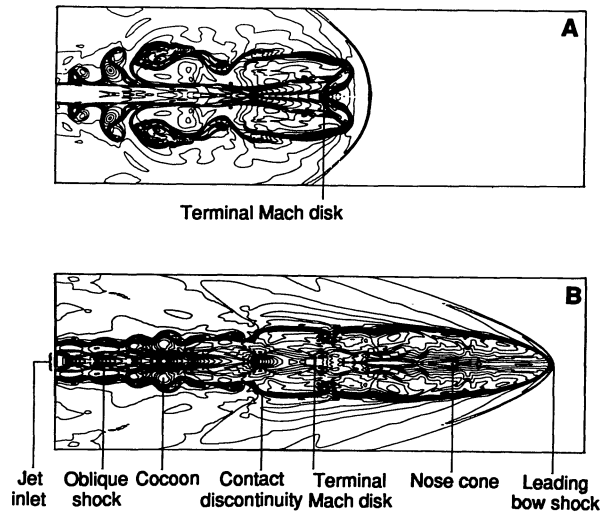

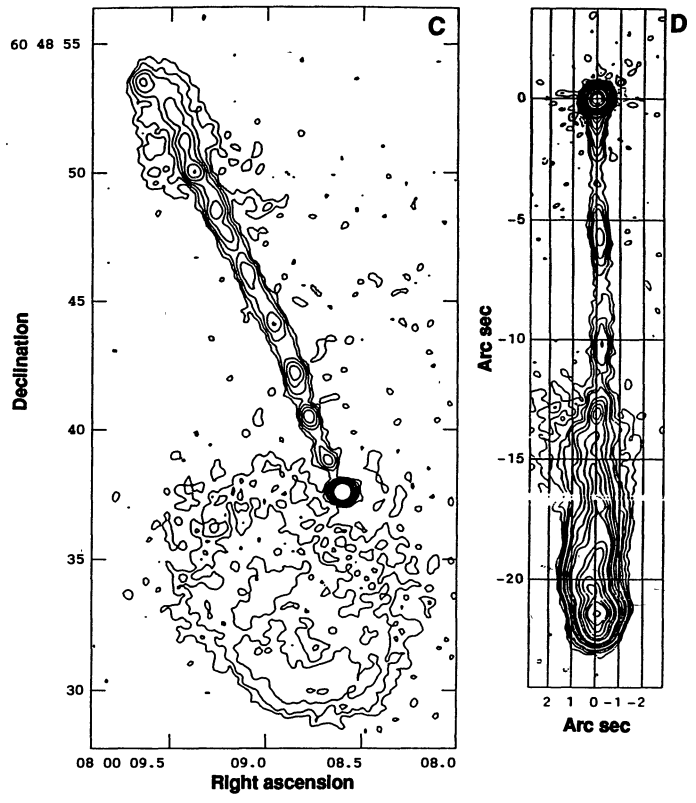

Fig. 3. Numerical model (**B**) and observations (**C** and **D**) of candidate magnetically confined, lobeless jet sources. (**A**) A simulation of a hydrodynamic jet ($\beta \gg 1$) with the same parameters as in Fig. 2. (B) is an MHD jet that is similar to (A) except $\beta < 1$. [Reprinted from Clarke *et al.* (1986) (*24*) with permission of the *Astrophysical Journal*] Note that (B) differs from (A) in the absence of a cocoon and the presence of a nose cone forward of the terminal Mach disk. Compare (B) with two MHD VLA jet candidates jets in (C) and (D) from (*26*).

candidate is the jet in the quasar 0800+608 (*26*). Relativistic beaming could also contribute in producing these lobeless, highly one-sided morphologies. If these sources are very close to the line of sight, such beaming effects could hide the counterjets and produce large contrasts between the beamed jets and the unbeamed lobes. However, the unusual spectral index gradient in 3C 273 is consistent with active magnetic fields as the agent responsible for the lobeless jet structure.

When the magnetic field is dynamically passive ($\beta \gg 1$), it is still necessary to evolve the field self-consistently in order to produce total intensity and polarization images of the radio source. Because the ZEUS code does not yet contain a relativistic gas component, we assume that the fast electrons are in energy equipartition with the thermal gas. Thus, the synchrotron emissivity is taken to be

$$\iota \propto P(B \sin \psi)^{3/2} \quad (5)$$

where ψ is the angle between the local **B** field and the line of sight. We then assume that the resulting emissivities are cylindrically symmetric and we integrate these emissivities along the line of sight to produce synchrotron surface brightness images. The resulting images are functions of both the angle of the jet axis with respect to the line of sight and the pitch angle of the magnetic field. Similarly, Stokes linear polarization parameters Q and U are calculated to produce images of the polarized intensity, fractional polarization, and projected magnetic field.

An example of one such theoretical emission map compared with a VLA image of 3C 219 is shown in Fig. 4 (*24, 27*). There is good agreement between many of the total intensity and polarization features. For example, both images show a circumferential pattern of projected magnetic field near the head of the source. This is a consequence of viewing a toroidal **B** field at an angle significantly out of the plane of the sky. Others (*28*) have found that a similar pattern of **B**-field vectors can be produced by the injection of an initially random **B** field. The important point is that in either case dynamical evolution of the jet (and thus compressing and shearing of the **B** field) strongly modifies the initial magnetic field pattern. Both maps in Fig. 4, A and B, also show partial jets that do not extend all the way from the jet inlet to the lobe. The **B** field in both the observations and the model changes orientation by 90° and decreases in fractional polarization in the transition region between the end of the visible jet and the lobe. These simulations suggest that the jet is initially bright as a result of the presence of biconical shocks near the inlet, but the surface brightness fades relative to the cocoon as these shocks become less prominent. Thus, the synchrotron emission image can give the appearance of a partial jet while the density and pressure distributions indicate a complete jet. This outcome emphasizes the importance of producing theoretical emission images from numerical simulations for comparison with radio images.

Born-Again Radio Jets

Magnetic field and emissivity effects may be responsible for the partial jets seen in some extragalactic sources such as 3C 219. Another possibility is that the jet outflow may be intermittent. Strong variability in the flux densities of compact cores associated with AGNs has been observed for many years. Some of these same sources reveal the presence of new radio knots at milliarc second scales after flux density outbursts from the core (*9*). This result seems to suggest an unsteady output of directed plasma between the core and the extended structure.

We have modeled the effects of a restarting jet by turning a beam on, then off, and then on again (in equal intervals), using the ZEUS code (*29*). Of particular interest is the impact of this intermittency on the jet and lobe morphologies. One epoch during the "born-again" phase is shown in Fig. 4C. Because the restarting jet propagates through the hot rarefied cocoon material of the original jet, it will be denser than the immediate surroundings and will advance ballistically. Thus, partial jets are short-lived relative to the original jet. For this simulation, the jet was in the partial phase for about one-third of the duty cycle. This fraction can be decreased and made consistent with current observed jet statistics if η is <0.01 (*29*).

This model also predicts that the lobe with the currently active jet will have a brighter, more compact hot spot than the lobe without a jet. The lobe with the jet will have a high surface brightness Mach disk (hot spot) at the extremity. On the other hand, without the momentum flux of the jet, the high-pressure hot spot will quickly

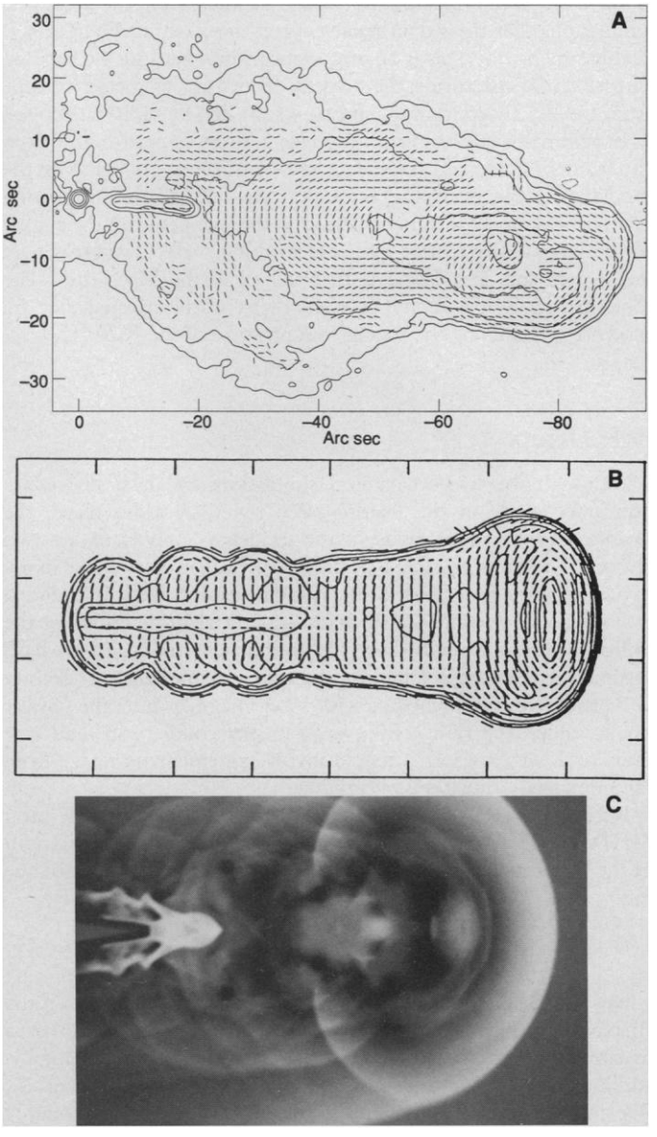

Fig. 4. Observations and models of partial jets in classical double sources. (**A**) The southern lobe of 3C 219 from (*27*) rotated counterclockwise by 45°; the dashed lines represent polarization magnetic field vectors. (**B**) The theoretical synchrotron image with overlaid magnetic field vectors for an MHD jet with a passive B field (that is, $\beta < 1$), a jet inclination of 60° with respect to the line of sight, and a magnetic field pitch angle of 30°. Note the excellent agreement in total intensity and magnetic field morphologies between (A) and (B). (**C**) An alternative model for a partial jet produced by a restarting beam; this is a gray scale image of the thermal pressure. [Reprinted from (*29*) with permission of the *Astrophysical Journal*]

expand, and its brightness will decrease rapidly. Such a jet–hot spot correlation is observed in many classical doubles (*30*).

Finally, a weak bow shock just in front of the restarted jet may be present within the jet channel if some radiating electrons remain. Although we see no evidence of a bow shock for 3C 219, there are indications of such a structure in at least one other source, 3C 33.1 (*29*).

The Dentist Drill Model

In a number of luminous radio galaxies and quasars, recent VLA images (see Fig. 5) reveal jets that are initially very straight and then curve dramatically into the radio lobes (*7, 8, 31*). In some instances, multiple hot spots are seen in these same lobes. Clearly, the standard axisymmetric jet model cannot accommodate this structure.

Several years ago, Scheuer (*32*) suggested that beams from AGNs may not always be perfectly straight but might have some jitter, much like a drill in the hands of an unsteady dentist. Such a "dentist drill" could be produced by precession of the beam originating within the galaxy nucleus (*33*) or by the formation of a hot spot cavity that bursts and redirects the beam flow (*34*). This dentist drill model could potentially explain some of the source asymmetries such as multiple hot spots corresponding to multiple jet working surfaces.

Recently, Hardee and Norman (*35*) have explored another hydrodynamical origin for jet jitter. They note that these jet-lobe structures might arise naturally when the artificially imposed axisymmetry of previous 2-D numerical models is relaxed. In 2-D numerical simulations, one accomplishes this by using a slab geometry in which the jet axis is allowed to move freely in the plane of the simulations and the jet is assumed to be infinitely wide along the orthogonal direction (that is, perpendicular to the computational plane). A perturbation on the initial velocity (either a step function or a driven sinusoid) is imposed with an amplitude in the direction perpendicular to the jet axis that is 1% of the bulk velocity. This, in turn, excites a series of surface and body wave modes that grow (initially) exponentially in amplitude (*36, 37*). The slab jet, as shown in Fig. 5, is observed to oscillate in the plane of the simulation as a result of the nonlinear amplification of the initial perturbation by the K-H kink mode instability. The observed jet "flapping" is driven by turbulent vortices in the lobe.

Such fluid instabilities, which must be present at some level in all jets, are a natural explanation of the beam jitter assumed to be present in the original dentist drill model. In addition, the jet flapping creates a pattern of filaments through a variety of hydrodynamic mechanisms such as shock excitation and ambient medium entrainment. This may explain the elaborate filamentary structure seen in the lobes of many extragalactic radio sources (*2, 38*).

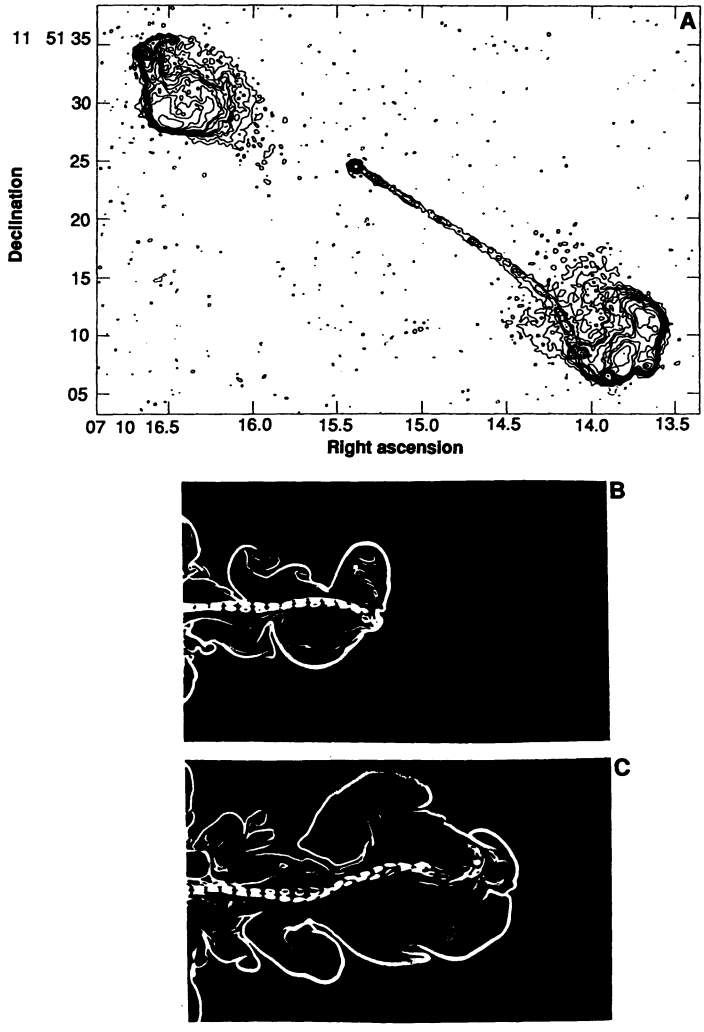

Fig. 5. Observations and models of jets that display Kelvin-Helmholtz fluid instabilities. (**A**) A VLA image of 3C 175 (*7*). (**B** and **C**) Emissivity images of a numerical jet simulation with slab symmetry (*35*). Gray scale representations of synchrotron emissivity are displayed in (B) and (C), which is computed as follows. Passive magnetic field loops are injected at the inlet which are subsequently advected through the flow by solving the magnetic induction equation. Although flux loops do not represent the true magnetic field structure in radio jets, they are excellent "tracer particles" to probe the jet velocity and shear fields.

Disruption of Radio Jets

In rich clusters of galaxies, radio sources known as wide-angle tails (WATs) are identified with dominant galaxies found at the cluster centers (*39*). The jets in these sources (Fig. 6A) are initially very straight but suddenly flare or disrupt (and usually bend) in the outer galaxy halo (typically 10 to 50 kpc from the nucleus). The jets evolve into diffuse, edge-darkened tails. In analogy to what is seen in the laboratory (*40*), one could interpret the jets as moderately supersonic (M = 2 to 5) fluid flows, and the tails as subsonic plumes that are subject to turbulent broadening and entrainment of the ambient medium. It is clear that the abrupt transition from jet to lobe cannot be produced in a smoothly varying external atmosphere. One concludes that there must be a corresponding abrupt change in the external pressure that results in the rapid decollimation of the jet.

We hypothesize that this "pressure wall" is produced at the interface between the ISM and the IGM. It may result, for example, from a supersonic wind originating in the AGN, contacting the static IGM and producing a standing shock. To test our idea, we propagated a mildly supersonic, light jet into an external medium with a standing shock (*41*). As the jet penetrates the external shock, a Mach disk is produced inside the jet (see Fig. 6B). This causes the jet to become subsonic and expand to reach thermal pressure balance with the surrounding ambient medium according to Bernouilli's theorem. The subsonic tail becomes turbulent and entrains significant amounts of ambient gas. For the jet to disrupt, its Mach number (relative to the jet sound speed) must be less than that of the wind (relative to the ambient sound speed). Our numerical simulations show a qualitative resemblance to WATs. If our model is correct, then a new gaseous component in central cluster galaxies (that is, the shock) has been detected by its effect on radio sources. This result illustrates that extended, moderate luminosity radio emission may be a sensitive tracer of the surrounding environment, capable of probing the hot IGM with higher resolution and

sensitivity than is possible with current x-ray telescopes.

In some galaxy clusters, the central IGM density is high enough that significant bremsstrahlung and spectral line cooling can occur on time scales much shorter than the cluster age. This cooling causes the central pressure to drop, and the resulting pressure gradient across the cluster drives a "cooling inflow" onto the central dominant galaxy. This flow may have a significant effect on extended radio emission generated by the central AGN, especially if the IGM flow becomes transonic near the galaxy core (typically ~1 kpc out from the galaxy center). At the sonic radius, the thermal pressure

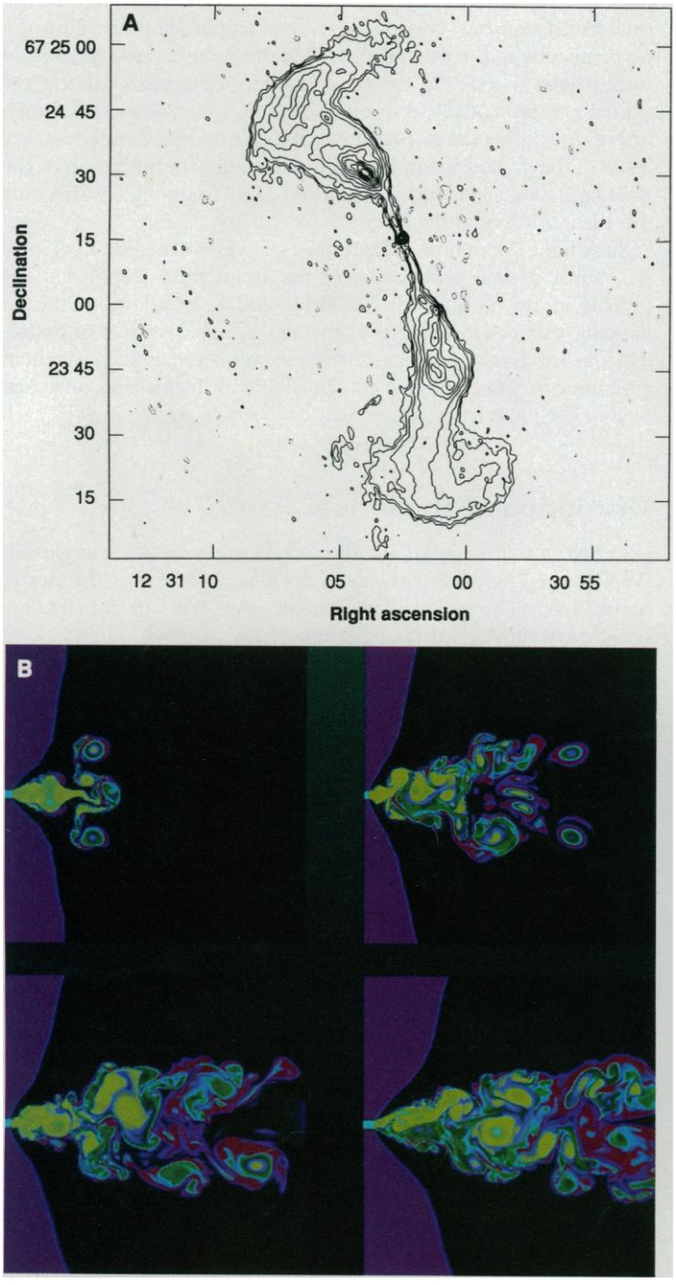

Fig. 6. Observations and models of a disrupting jet in a wide-angle tailed radio galaxy. (**A**) A VLA image of the radio source 1231 + 674 in the rich Abell cluster 1559 [O'Donoghue *et al.* (*39*)]. (**B**) Density images of the evolution of a slab symmetric jet with $\eta = 0.01$ and $M = 2.5$ passing through a shock in the ambient medium (*41*). Note the sudden transition from a well-collimated jet to a subsonic, turbulent tail.

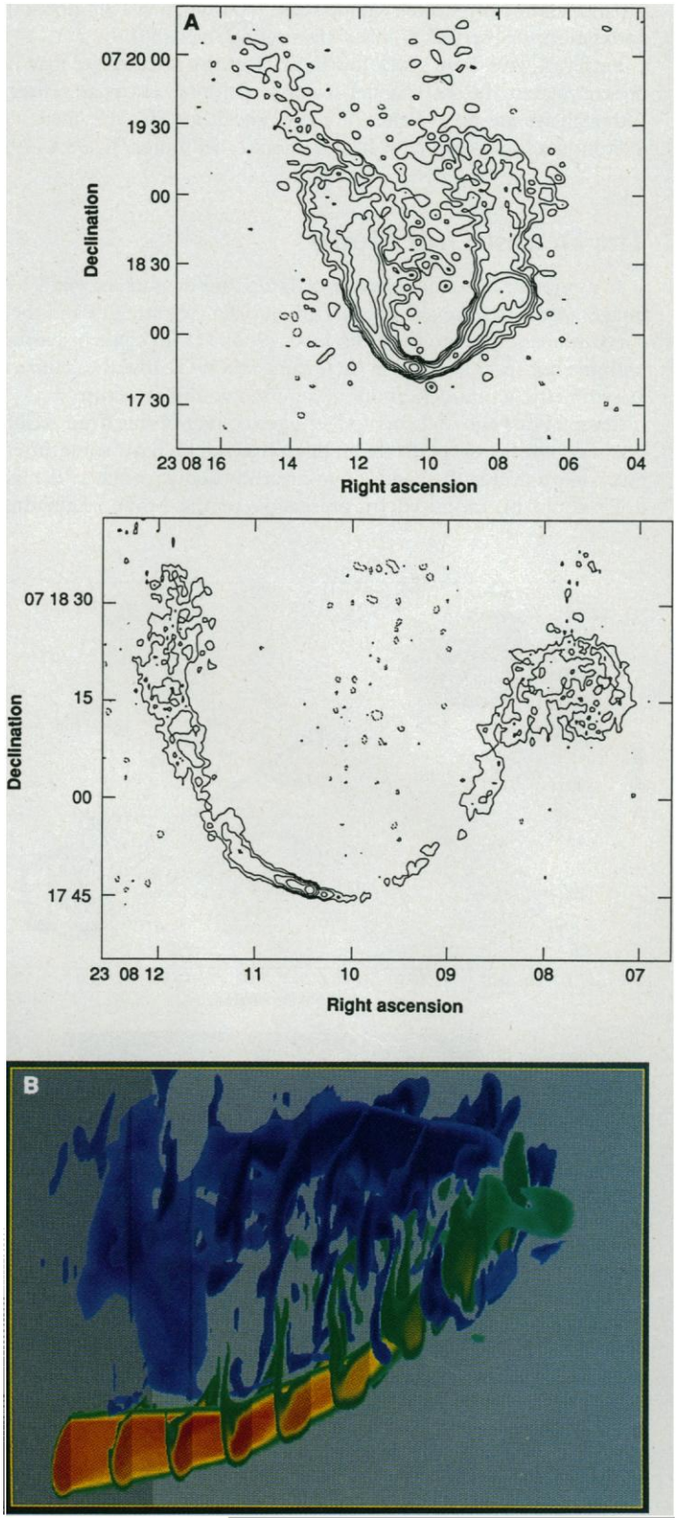

Fig. 7. Observations and models of narrow-angle tailed radio galaxies. (**A**) Two VLA images of NGC 7503 in a poor cluster of galaxies (*47*); the U-shaped jets-tails are produced by dynamical pressure resulting from motion through an IGM. (**B**) An image of a 3-D simulation of a supersonic jet bent by a transonic cross wind (*34*). The longitudinal velocity components on orthogonal slice planes passing through the jet are displayed. The jet cross section is initially circular but is subsequently flattened as ram pressure bends the jet. Thus, a bent jet becomes a ribbon. Rayleigh-Taylor instabilities split this ribbon into filaments leading to jet disruption.

drops precipitously from the outer to the inner parts of the galaxy. Numerical models demonstrate that the resulting pressure wall produces an effect similar to that above in which a shock forms within the jet, causing the jet to disrupt (*36*). This finding is significant because there is a class of relatively compact, amorphous, small jet or jetless sources associated with cooling flow clusters (*36, 42*). Thus, once again, it would appear that the surrounding medium plays an important role in shaping moderate luminosity sources in galaxy clusters.

Numerical Simulations in Three Dimensions

The 2-D simulations we have described thus far have been an extremely useful source of insight on jet structure, dynamics, and stability. Many of the lessons learned in two dimensions should carry over to three dimensions relatively unchanged. However, the detailed interpretation of many radio morphologies, such as hot spot structure, bent jets, and filamentary radio lobes can only be made on the basis of fully 3-D simulations. Heretofore, such simulations were out of reach because of limitations in the computer memory and speed. Today, thanks to the availability of large memory supercomputers such as the Cray-2 at Illinois, we can proceed. During the past 2 years, our group has begun modeling radio galaxies in three dimensions with encouraging initial results. Clarke, Stone, and Norman (*43*) have simulated the standard model of classical doubles in three dimensions and confirmed the existence of all of the features found in the axisymmetric simulations (compare Figs. 1 and 2) at early epochs. As the jet continues to evolve, it begins to flap just as the slab jet does (see Fig. 5). Thereafter, the termination shock structures bear little resemblance to the Mach disk present at earlier times. In addition, strong eddies develop in a plane perpendicular to the jet axis, confirming an earlier result of Arnold and Arnett (*19*). We are currently in the process of repeating this simulation with the addition of passive tangled magnetic fields so that we may perform numerical observations of the resultant hot spot and radio lobe.

A problem that can only be studied in three dimensions is the interaction of a supersonic jet with a transonic cross wind, a situation that occurs commonly for tailed radio galaxies in clusters. A jet emerging from an AGN in such a cluster will be swept back into a "U" shape by virtue of the galaxy's relative motion through the dense IGM (*44*). This widely accepted explanation for tailed radio sources has scarcely been investigated in detail numerically (*45*). Questions of interest are (i) how does a supersonic jet bend, (ii) through what angle can a supersonic jet be bent and remain stable, and (iii) what mechanism is responsible for the sudden flaring and disruption of bent jets into diffuse radio tails? Figure 7B (*34*) provides a glimpse of the complexity of such flows and partial answers to these questions. It appears that the jet bends in a series of discrete steps mediated by oblique internal shock waves. Behind each shock is a high-pressure knot; thus a bent jet should be knotty. This is consistent with high-resolution observations of tailed radio galaxies such as NGC 1265 (*46*) and NGC 7503 in Fig. 7A (*47*). Another interesting finding is that the jet is disrupted by Rayleigh-Taylor instabilities along its upwind edge, which effectively splits the jet into strands. These strands then quickly become unstable to the K-H instability and lose coherence, producing a turbulent tail.

Concluding Remarks

Although the results of the numerical simulations described in this review are beginning to produce some important insights into the physics of radio jets, it is important to take note of the limitations of current models. For example, ZEUS and other similar codes allow only nonrelativistic bulk flow at present. Relativistic effects can alter the appearance of the jets and lobes, amplify jet bending, and modify the radiative properties of shocks. Relativistic bulk motion is clearly important on the smallest scales (*9*) and could be important for large-scale jets in luminous sources. Another limitation is the lack of microphysics in the models. Nonadiabatic synchrotron losses and thermal cooling of relativistic electrons may be energetically important in extended radio lobes and tails where the spectral index is steep (although not as important in compact features such as hot spots). In addition, in situ particle acceleration via shocks or turbulence (*25*) may be important in altering the energetics of electrons and the observed spectra of sources. Current numerical models address the evolution of the magnetic fields but not the particle energy distribution.

Nonetheless, with the advent of 3-D modeling, we are entering into an exciting era that offers further promise to explain the rich variety of complex features seen on radio maps. As the memory and speed of supercomputer class machines continue to improve over the next decade, these other important pieces of physics will be added to codes such as ZEUS. Taken together, aperture synthesis and supercomputer observations will be powerful probes of the origin and evolution of extended extragalactic radio sources.

REFERENCES AND NOTES

1. A. R. Thompson, B. G. Clark, C. M. Wade, P. J. Napier, *Astrophys. J. Suppl. Ser.* **44**, 151 (1980).
2. R. A. Perley, J. W. Dreher, J. J. Cowan, *Astrophys. J.* **285**, L35 (1984); A. H. Bridle and R. A. Perley, *Annu. Rev. Astron. Astrophys.* **22**, 319 (1984).
3. See, for example, A. G. Pacholczyk, *Radio Astrophysics* (Freeman, San Francisco, 1970); N. Kardashev, *Sov. Astron. AJ* **89**, 217 (1966).
4. B. L. Fanaroff and J. M. Riley, *Mon. Not. R. Astron. Soc.* **167**, 31P (1974).
5. Original analytical models were proposed by R. D. Blandford and M. J. Rees [*ibid.* **169**, 395 (1974)] and P. A. G. Scheuer [*ibid.* **166**, 513 (1974)]. For more recent reviews, see M. C. Begelman, M. J. Rees and R. D. Blandford [*Rev. Mod. Phys.* **56**, 255 (1984)] and D. S. De Young [*Science* **252**, 389 (1991)].
6. One can show that the ratio of the jet to counterjet flux densities for a relativistically beamed jet is

$$\frac{S_j}{S_{cj}} = \left(\frac{1 + \beta_j \cos\theta}{1 - \beta_j \cos\theta}\right)^{2+\alpha}$$

where $\beta_j = V_j/c$, c is the speed of light, θ is the angle of the jet axis with respect to the line of sight, and α is the spectral index as defined in the text. For example, for $\beta_j = 0.99$, $\alpha = 0.5$, and $\theta = 20°$, large contrasts between the jet and counterjet surface brightness can occur ($S_j/S_{cj} \approx 4000$). See P. A. G. Scheuer and A. C. S. Readhead, *Nature* **277**, 182 (1979).
7. A. H. Bridle, D. H. Hough, J. O. Burns, R. A. Laing, C. J. Lonsdale, in preparation.
8. I. Fernini, J. P. Leahy, J. O. Burns, J. P. Basart, *Astrophys. J.*, in press.
9. J. A. Zensus and T. J. Pearson, Eds., *Parsec-Scale Radio Jets* (Cambridge Univ. Press, New York, 1990).
10. W. Forman and C. Jones, *Annu. Rev. Astron. Astrophys.* **20**, 547 (1982).
11. R. V. E. Lovelace, *Nature* **262**, 649 (1976).
12. D. S. De Young, *Astrophys. J.* **307**, 62 (1986).
13. See, for example, L. D. Landau and E. M. Lifshitz, *Fluid Mechanics* (Pergamon, New York, 1982).
14. D. A. Clarke, thesis, University of New Mexico (1988).
15. M. L. Norman and K.-H. A. Winkler, Eds., *Astrophysical Radiation Hydrodynamics* (Reidel, Dordrecht, 1986), vol. c188, p. 187.
16. C. Evans and J. F. Hawley, *Astrophys. J.* **332**, 659 (1988).
17. J. M. Stone, thesis, University of Illinois at Urbana-Champaign (1990); _____ and M. Norman, in preparation.
18. M. L. Norman, L. Smarr, K.-H. A. Winkler, M. D. Smith, *Astron. Astrophys.* **113**, 285 (1982); M. J. Wilson and P. A. G. Scheuer, *Mon. Not. R. Astron. Soc.* **205**, 449 (1983); A. G. Williams, thesis, Cambridge University (1985); D. Kössl and E. Müeller, *Astron. Astrophys.* **206**, 204 (1988).
19. C. N. Arnold and W. D. Arnett, *Astrophys. J.* **305**, L57 (1986).
20. Light jets with high Mach numbers are not inconsistent with our assumption of nonrelativistic bulk flow. For example, a jet with $M = 10$ and sound speed 3000 km s^{-1} (corresponding to a jet temperature of 6×10^8 K) has a velocity of $0.1c$. Even lower velocities are possible for a given Mach number if the jet is cooler. Furthermore, the structure of mildly relativistic jets ($\gamma \leq 2$) is not greatly different from that of nonrelativistic jets (M. L. Norman, unpublished simulations).
21. Observations of overpressured jets are reported in R. I. Potash and J. F. C. Wardle, [*Astrophys. J.* **239**, 42 (1980)] and J. O. Burns, J. P. Basart, D. S. De Young, and D. C. Ghiglia [*ibid.* **283**, 515 (1984)]. An analytical model for these jets is described in M. C. Begelman and D. Cioffi [*ibid.* **345**, L21 (1989)], and numerical

simulations are discussed by M. L. Norman [*Bull. Am. Astron. Soc.* **19**, 651 (1987)] and C. Loken, J. O. Burns, D. A. Clarke, and M. L. Norman, in preparation.
22. The classic reference in this field is S. Chandrasekhar, *Hydrodynamic and Hydromagnetic Stability* (Clarendon, Oxford, 1961); see also P. E. Hardee [*Astrophys. J.* **250**, L9 (1981)] and A. Ferrari, E. Trussoni; and L. Zaninetti [*Astron. Astrophys.* **79**, 190 (1979)].
23. M. L. Norman, K.-H. A. Winkler, L. Smarr, in *Physics of Energy Transport in Extragalactic Radio Sources, National Radio Astronomy Observatory Workshop No. 9* (NRAO, Green Bank, WV, 1984), p. 150.
24. D. A. Clarke, M. L. Norman, J. O. Burns, *Astrophys. J.* **311**, L63 (1986); *ibid.* **342**, 700 (1989); K. R. Lind, D. G. Payne, D. L. Meier, R. D. Blandford, *ibid.* **344**, 89 (1989).
25. A. R. Bell, *Mon. Not. R. Astron. Soc.* **182**, 147 (1978); R. Blandford and D. Eichler, *Phys. Rep.* **154**, 1 (1987).
26. The image of 3C 273 (Fig. 3D) is from R. A. Perley, unpublished data; images of 0800 + 608 (Fig. 3C) can be found in N. Jackson, I. W. A. Browne, D. L. Shone, K. R. Lind, *Mon. Not. R. Astron. Soc.* **244**, 750 (1990).
27. D. A. Clarke, A. H. Bridle, J. O. Burns, R. A. Perley, M. L. Norman, in preparation.
28. A. P. Matthews and P. A. G. Scheuer, *Mon. Not. R. Astron. Soc.* **242**, 616 (1990); *ibid.*, p. 623.
29. D. A. Clarke and J. O. Burns, *Astrophys. J.* **369**, 308 (1991); for the sample of 3CR sources with jets discussed in this paper, 10% have lobes with partial jets.
30. R. A. Laing, in *Lecture Notes in Physics No. 327, Hot Spots in Extragalactic Radio Sources* (Springer-Verlag, New York, 1989), p. 84.
31. P. D. Barthel, G. K. Miley, R. T. Schilizzi, C. J. Lonsdale, *Astron. Astrophys. Suppl. Ser.* **73**, 515 (1988).
32. P. A. G. Scheuer, in *International Astronomical Union Symposium 97, Extragalactic Radio Sources* (Reidel, Dordrecht, 1982), p. 163.
33. A. G. Williams and S. F. Gull, *Nature* **313**, 34 (1985).
34. D. Balsara, thesis, University of Illinois at Urbana-Champaign (1990).
35. P. E. Hardee and M. L. Norman, *Astrophys. J.* **342**, 680 (1989); *ibid.* **365**, 134 (1990).
36. J.-H. Zhao, thesis, University of New Mexico (1990).
37. ———, J. O. Burns, M. L. Norman, M. E. Sulkanen, in preparation.
38. Examples of filamentation in extended radio sources include: M 87 in D. C. Hines, F. N. Owen, J. A. Eilek, *Astrophys. J.* **347**, 713 (1989); Fornax A in E. B. Fomalont, K. A. Ebneter, W. J. M. van Breugel, R. D. Ekers, *ibid.* **346**, L17 (1989); Hercules A in J. Dreher and E. Feigelson, *Nature* **308**, 43 (1984).
39. J. O. Burns, *Can. J. Phys.* **64**, 373 (1986); A. A. O'Donoghue, F. N. Owen, J. A. Eilek, *Astrophys. J. Suppl. Ser.* **72**, 75 (1990).
40. J. W. Shirie and J. G. Seubold, *Am. Inst. Aeronaut. Astronaut. J.* **5** (no. 11), 2062 (1967).
41. M. L. Norman, J. O. Burns, M. Sulkanen, *Nature* **335**, 146 (1988).
42. J. O. Burns, *Astron. J.* **99**, 14 (1990).
43. D. A. Clarke, J. M. Stone, M. L. Norman, *Bull. Am. Astron. Soc.* **22**, 801 (1990).
44. Recent simulations by D. S. De Young [*Astrophys. J.* **371**, 69 (1991)] suggest that ram pressure bending of jets may be even more effective than that indicated by Euler's equation, which is generally used to describe jet bending and is given by

$$\frac{\rho_j V_j^2}{R_j} = \frac{\rho_{amb} V_g^2}{R_{amb}}$$

where R_j is the radius of curvature of the jet, ρ_{amb} is the density of the medium surrounding the jet, V_g is the galaxy velocity, and R_{amb} is the pressure scale height over which the ram pressure is effective. However, the numerical results might be affected by the large numerical viscosity inherent in De Young's code.
45. A. G. Williams and S. F. Gull, *Nature* **310**, 33 (1984).
46. C. P. O'Dea and F. N. Owen, *Astrophys. J.* **301**, 841 (1986).
47. D. Batuski, R. Hanisch, J. Burns, *Bull. Am. Astron. Soc.* **22**, 882 (1990).
48. This paper is based on an invited review talk presented at the 176th meeting of the American Astronomical Society held in Albuquerque, New Mexico, 1990. This research was supported by National Science Foundation grants AST-8611511 and AST-9012353, and National Aeronautics and Space Administration grant NAG8-747. We are grateful to our collaborators including P. Hardee, J.-H. Zhao, M. Sulkanen, J. Stone, D. Balsara, K.-H. Winkler, C. Loken, and L. Smarr for their contributions to this work. We also thank D. Batuski, I. Browne, A. Bridle, D. De Young, A. O'Donoghue, J. Eilek, F. Owen, and R. Perley for stimulating discussions and for the use of their data.

Rules of Language

STEVEN PINKER

Language and cognition have been explained as the products of a homogeneous associative memory structure or alternatively, of a set of genetically determined computational modules in which rules manipulate symbolic representations. Intensive study of one phenomenon of English grammar and how it is processed and acquired suggests that both theories are partly right. Regular verbs (*walk-walked*) are computed by a suffixation rule in a neural system for grammatical processing; irregular verbs (*run-ran*) are retrieved from an associative memory.

EVERY NORMAL HUMAN CAN CONVEY AND RECEIVE AN unlimited number of discrete messages through a highly structured stream of sound or, in the case of signed languages, manual gestures. This remarkable piece of natural engineering depends upon a complex code or grammar implemented in the brain that is deployed without conscious effort and that develops, without explicit training, by the age of four. Explaining this talent is an important goal of the human sciences.

Theories of language and other cognitive processes generally fall into two classes. Associationism describes the brain as a homogeneous network of interconnected units modified by a learning mechanism that records correlations among frequently co-occurring input patterns (*1*). Rule-and-representation theories describe the brain as a computational device in which rules and principles operate on symbolic data structures (*2, 3*). Some rule theories further propose that the brain is divided into modular computational systems that have an organization that is largely specified genetically, one of the systems being language (*3, 4*).

During the last 35 years, there has been an unprecedented empirical study of human language structure, acquisition, use, and breakdown, allowing these centuries-old proposals to be refined and tested. I will illustrate how intensive multidisciplinary study of one linguistic phenomenon shows that both associationism and rule theories are partly correct, but about different components of the language system.

Modules of Language

A grammar defines a mapping between sounds and meanings, but the mapping is not done in a single step but through a chain of intermediate data structures, each governed by a subsystem. Morphology is the subsystem that computes the forms of words. I focus on a single process of morphology: English past tense inflection, in which the physical shape of the verb varies to encode the relative time of occurrence of the referent event and the speech act. Regular

The author is in the Department of Brain and Cognitive Sciences, Massachusetts Institute of Technology, Cambridge, MA 02139.